

Selectivity Switching of CO₂ Hydrogenation from HCOOH to CO with an *In Situ* Formed Ru–Li Complex

Qiongyao Chen, Chaoren Shen, Gangli Zhu,* Xuehua Zhang, Chun-Lin Lv,* Bo Zeng, Sen Wang, Junfen Li, Weibin Fan, and Lin He*



Cite This: *ACS Catal.* 2021, 11, 9390–9396



Read Online

ACCESS |



Metrics & More



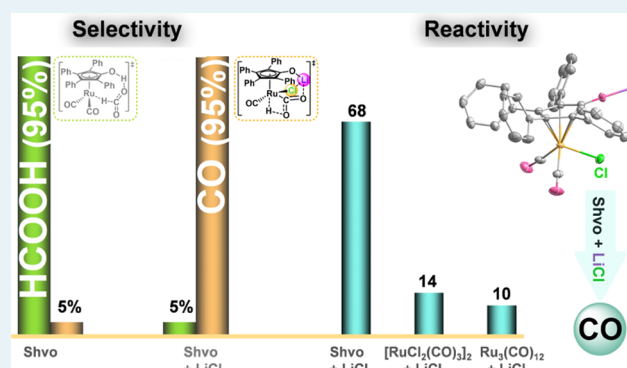
Article Recommendations



Supporting Information

ABSTRACT: Herein, we report the role of alkali halide salt in regulating the pathway of CO₂ hydrogenation in the presence of Shvo's complex. Particularly, the collaboration of Shvo's complex with LiCl exhibited as a highly efficient catalyst for CO₂ hydrogenation to CO instead of the kinetically favorable product HCOOH under mild conditions. The reaction can be initiated at 45 °C with CO as the dominant product, and the rate of CO formation was almost 80 times to that in the absence of LiCl at 60 °C. Under optimized conditions, the TON_{CO} could reach 1555 at 160 °C, much higher than the reported results of the most efficient Ru-based homogeneous catalyst. Density functional theory calculations demonstrated that the cooperation of the alkali cation and chloride anion contributed to reducing the energy barrier of CO₂ activation to form the key Ru–CO₂H intermediate. An *in situ* formed mixed Ru–Li complex (**5**) has been characterized by X-ray crystallography, highlighting the indispensability of electrostatic interactions between LiCl and Shvo's complex for enhanced reactivity and altered selectivity.

KEYWORDS: alkali metal salts, CO₂ hydrogenation, promoter effect, selectivity switch, Ru–Li complex.

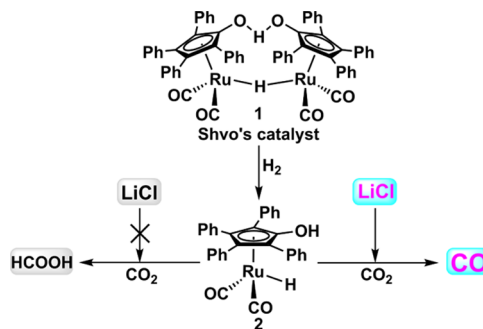


1. INTRODUCTION

Hydrogenation of CO₂ is a process with several possible channels, leading to various products, including HCOOH,¹ CO,² MeOH,³ and CH₄.⁴ Among these, direct hydrogenation of CO₂ to CO, the reverse water gas shift reaction (RWGS),⁵ offers a promising approach to access the sustainable source for synthesis gas.⁶ Despite its utility, the procedure often demands harsh conditions (>160 °C in most cases) and suffers from competition with other reaction pathways.⁷ Moreover, under mild conditions, CO formation is kinetically disfavored compared with HCOOH formation.⁸ This situation becomes more significant to homogeneous catalysts with ligands bearing O–H/N–H groups as the hydrogen-bonding interaction between the functional groups and the oxygen of CO₂ is beneficial to generate the formate (MO₂CH) intermediate.⁹ Thus, the prediction regarding the chemoselectivity of CO₂ hydrogenation catalyzed by hydroxycyclopentadienyl metal complexes (including Shvo's catalyst **1**) gives HCOOH instead of CO as the default product,¹⁰ although experimentally, these types of catalysts for CO₂ hydrogenation were unexplored prior to this report.

In the present work (Scheme 1), the capability of Shvo's catalyst for hydrogenating CO₂ to HCOOH was confirmed. More intriguingly, adding LiCl can switch the selectivity of the product toward CO even at extremely low temperatures (45–

Scheme 1. Selectivity Switching of CO₂ Hydrogenation

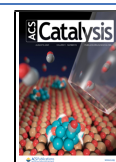


60 °C). Under the optimized conditions, the TON_{CO} could reach 1555 at 160 °C, much higher than that of state-of-the-art Ru-based homogeneous catalytic systems. Density functional theory (DFT) calculations validated the contribution of Li⁺

Received: April 26, 2021

Revised: June 23, 2021

Published: July 13, 2021



and Cl^- in reducing the formation energy of the MCO_2H intermediate for RWGS. A Ru–Li complex (**5**) formed *in situ* has been characterized by X-ray crystallography, revealing the substitution of the acidic proton on the hydroxycyclopentadienyl ligand and carbonyl ligand on the Ru center respectively with Li^+ and Cl^- . This is an unusual example supported with crystallographic evidence that clarifies the coexistence of the alkali cation and chloride anion in prompting the catalytic reactivity and altering the reaction pathway.

2. EXPERIMENTAL DETAILS

2.1. Catalyst Synthesis. For the synthesis of Shvo's catalyst, complexes **2**, **3**, and **4** were synthesized according to the previous reports. Detailed procedures are in Section 2 of the Supporting Information.

2.1.1. Synthesis of Complex 5. A 50 mL autoclave was charged with Shvo's catalyst (271 mg, 0.25 mmol) or complex **2** (271 mg, 0.5 mmol), LiCl (43 mg, 1 mmol), *N*-methyl-2-pyrrolidone (NMP, 2 mL), and a magnetic stirring bar. At room temperature, the autoclave was flushed with N_2 three times. Then, the pressure of N_2 was charged up to 1 MPa. The reaction mixture was heated at 120 °C for 5 h. Afterward, the autoclave was cooled to room temperature, and the residue gas was slowly released. 2–3 mL of CH_2Cl_2 was added to the reaction solution, and the reaction mixture was filtered off. Then, hexane was added into the filtrate, and the resulting pale-yellow powder **5** was filtered off (261 mg, 83%). Single crystals were cultivated by the liquid–liquid diffusion technique via layering the CH_2Cl_2 solution with hexane. ^1H NMR (CDCl_3 , 400 MHz): δ 7.40–7.42 (m, 4H), 7.19–7.21 (m, 6H), 7.11 (m, 2H), 7.0–7.04 (m, 4H), 6.90–6.93 (m, 4H), 3.36 (t, $J = 7.1$ Hz, 2H), 2.81 (s, 3H), 2.33 (t, $J = 8.1$ Hz, 2H), 1.95–2.03 (m, 2H). ^{13}C NMR (CD_3OD , 100.6 MHz): δ 201.00, 176.34, 133.50, 132.44, 132.01, 131.43, 130.81, 127.46, 127.02, 126.97, 125.92, 101.16, 82.57, 49.46, 30.31, 28.42, 17.18. HRMS-ESI (m/z): $[\text{M} - \text{H}]^-$ calcd for $\text{C}_{31}\text{H}_{20}\text{ClO}_3\text{Ru}^-$, 577.0155; found, 557.0173.

2.2. General Procedures for the CO_2 Hydrogenation Process. The following procedure for CO_2 hydrogenation reactions can be considered representative. A 100 mL Parr autoclave was charged with the Ru-based catalyst (0.05 mmol), the additive (0.1 mmol), the solvent (1 mL), and a magnetic stirring bar. At room temperature, the autoclave was flushed with carbon dioxide three times. Then, CO_2 was charged up to 3 MPa, followed by charging H_2 to obtain a total pressure of 6 MPa. The reaction mixture was heated at 120 °C for 10 h. Afterward, the autoclave was cooled to room temperature. Gas products were collected by gas sampling bags after reaction and were analyzed by gas chromatography equipped with a thermal conductivity detector (TCD) and flame ionization detector (FID). TON_{CO} of gaseous products was determined based on the gas chromatography (GC) analysis results. Gas products were analyzed using FID with a methanizer or TCD for CO. The liquid product (HCOOH) was determined by ^1H NMR with *N,N*-dimethylformamide (DMF) as an internal standard. The concentration of gaseous products was quantified by the integral area ratio of the reduction products to the standard gas. TON_{CO} of gaseous products were calculated by the following equations:

$$V_{\text{CO}} \% = \frac{A_1}{A_s} \times 0.5006\% \text{ GC a} \quad (1)$$

$$V_{\text{CO}} \% = \frac{A_1}{A_s} \times 2\% \text{ GC b} \quad (2)$$

$$\text{TON}_{\text{CO}} = \frac{PV}{RT \times n_{\text{Ru}}} \times V_{\text{CO}} \% \quad (3)$$

where A_1 is the peak area of CO, A_s is the peak area of the standard gas with $V_{\text{CO}} \%$ equal to 0.5006% or 2%, $V_{\text{CO}} \% \leq 1$ vol % [GC a], $V_{\text{CO}} \% \geq 1$ –3 vol % [GC b], P is the total pressure of the Parr autoclave (Pa), V is the total volume of the Parr autoclave (m^3), $T = 298$ (K), $R = 8.314$ J/(mol·K), and n_{Ru} is the mole of the metal (mol).

2.3. In Situ Formation of Intermediate 5 under the Optimal Conditions. The 100 mL Parr autoclave was charged with Shvo's catalyst (135 mg, 0.125 mmol), LiCl (0.5 mmol), NMP (1.5 mL), and a magnetic stirring bar. At room temperature, the autoclave was flushed with CO_2 three times. Then, CO_2 was charged up to 3 MPa, followed by charging H_2 to obtain a total pressure of 6 MPa. The reaction mixture was heated at 120 °C for 1 h. After cooling to room temperature, the residue gas was slowly released. CH_2Cl_2 (ca. 2–3 mL) was added into the reaction solution, and the reaction mixture was filtered off. Single crystals were cultivated by the liquid–liquid diffusion technique via layering the CH_2Cl_2 solution with hexane. After 3 days, light-yellow crystals were obtained. The results of X-ray crystallographic characterization show that complex **5** also exists under the reaction conditions.

2.4. Procedures for Investigating the Active Ru–H Species. **2.4.1. Evidence for the Interaction between LiCl and Shvo's Catalyst.** After reaction in anhydrous THF under 6 MPa of H_2 at 120 °C for 10 h, Shvo's catalyst was transformed to the mixture of Ru–H complexes. The ^1H NMR spectra of this mixture containing Ru–H complexes displayed two resonance signals at –9.87 and –10.13 ppm (the procedure was identical to the procedure of preparing complex **2** except changing the temperature to 120 °C). The resonance signal at –9.87 ppm can be attributed to complex **2**.

To investigate the interaction between LiCl and Shvo's catalyst, the following operation was performed in a glovebox with N_2 gas protection. An NMR tube was charged with the mixture of Ru–H complexes (20 mg) and anhydrous CDCl_3 (600 μL). Then, LiCl (3 mg) dissolving in NMP (200 μL) was subjected to the NMR tube. The reaction between complex **2** and LiCl proceeds fast enough under ambient conditions. This solution was characterized by ^1H NMR as quickly as possible.

2.4.2. Investigating the Evolution of Complex 5 under 6 MPa H_2 and under Optimized Reaction Conditions. All the following operations were conducted in a glovebox with N_2 gas protection. A 50 mL autoclave was charged with Ru complex **5** (174 mg, 0.1 mmol), NMP (2 mL), and a magnetic stirring bar. At room temperature, the autoclave was flushed with H_2 three times. Then, the pressure of H_2 was charged up to 6 MPa. The reaction mixture was heated at 120 °C for 1 h. After cooling the autoclave to room temperature, the residual gas was slowly released. Then, the autoclave was transferred into a glovebox with N_2 gas protection. 100 μL of NMP solution of the reaction mixture was subjected to an NMR tube charged with 600 μL of CDCl_3 for ^1H NMR analysis. The above-mentioned experimental procedure was repeated, except that 3 MPa CO_2 together with 3 MPa H_2 instead of 6 MPa H_2 was charged to confirm the Ru–H species under reaction conditions.

2.5. Computational Methods. All the calculations presented in this work were carried out with the Gaussian 16 software package.¹¹ The structures of reactants, intermediates, and products as well as transition states were optimized using the B3LYP hybrid-GGA functional, in combination with the LANL2DZ basis set¹² for Ru atoms and the 6-31G(d, p) basis set for rest atoms (BS1). Vibrational frequencies of each stationary structure were analyzed at the same level of theory to characterize the nature of the stationary points as local minima and give the thermal correction to Gibbs free energy. The minimum-energy path was obtained using intrinsic reaction coordinate calculations to confirm the connection of each transition state with the designated equilibrium species. In addition, the implicit solvation of *N,N*-dimethylacetamide has also been considered. Single-point energy calculations have been performed using the polarized continuum model with the SMD-Coulomb atomic radii¹³ for the united atom topological model at the B3LYP level based on each optimized geometry, with the SDD basis set¹⁴ for Ru atoms and the 6-311+G(d,p) basis set for rest atoms, denoted as B3LYP-SCRF(SMD)/BS2.

3. RESULTS AND DISCUSSION

The investigation started from evaluating the catalytic performance under CO₂ (3 MPa) and H₂ (3 MPa) at 60 °C for 10 h (Table 1). The activity of Shvo's catalyst for CO₂ hydrogenation was confirmed (entry 1). By adding different alkali chloride salts, the major product of CO₂ hydrogenation

Table 1. Influence of Alkali Halides on the Selectivity of CO₂ Hydrogenation^a

entry	salt	temp. (°C)	CO ₂ + H ₂ $\xrightarrow[\Delta]{\text{Shvo's catalyst}}$ CO + H ₂ O		TON		sel. (%)	
			<i>n</i> (μmol)		CO	FA	CO	FA
			CO	FA	CO	FA	CO	FA
1	none	60	6.5	123.9	~0	2	5	95
2	LiCl	60	486.9	40.7	10	1	95	5
3	NaCl	60	204.5	71.9	4	1	74	26
4	KCl	60	156.7	67.3	3	1	70	30
5	CsCl	60	221.0	54.5	4	1	80	20
6	LiF	60	28.8	55.0	1	1	35	65
7	LiBr	60	254.7	132.6	5	3	66	34
8	LiI	60	7.2	205.0	~0	4	3	97
9	LiCl	45	167.0	64.0	2	1	67	33
10	LiCl	80	1271.3	52.9	25	1	96	4
11	LiCl	100	3385.5	trace	68		>99	
12	LiCl	120	4442.4	trace	89		>99	
13 ^b	LiCl	120	N.D.	N.D.				
14 ^c	LiCl	120	4928.8	trace	99		>99	
15 ^d	LiCl	120	2886.3	trace	115		>99	
16 ^e	LiCl	120	579.1	trace	290		>99	
17 ^f	LiCl	140	992.7	N.D.	496		>99	
18 ^f	LiCl	160	3110.2	N.D.	1555		>99	

^aReaction conditions: 0.025 mmol Shvo's catalyst, 0.1 mmol salt, 1 mL of NMP, 3 MPa CO₂ and 3 MPa H₂, 10 h. *n*_{HCOOH} is determined by ¹H NMR with DMF as an internal standard. ^bWithout Shvo's catalyst. ^c4 MPa CO₂ and 4 MPa H₂. ^d0.0125 mmol Shvo's catalyst and 0.05 mmol salt. ^e0.001 mmol Shvo's catalyst and 0.004 mmol salt. ^f0.001 mmol Shvo's catalyst. N.D. = not detected. FA = formic acid. All results represent the average values for the results of three runs.

was switched from HCOOH to CO (entries 2–5). Among the salts tested, LiCl performed best in the low-temperature hydrogenation of CO₂ to CO. With the addition of 2 equiv LiCl, the selectivity toward CO increased from 5 to 95%. Correspondingly, the RWGS activity was elevated by almost 2 orders of magnitude compared to the system without adding the salt (480 vs 6 μmol). Of alkali halide salts other than LiF and LiI, LiBr also manifested a significant positive effect on facilitating CO generation (entries 6–8). The observed subtle promoting effect of halides is probably attributed to the solubility of lithium halide and the coordination of the halide anion to Ru. RWGS can be initiated at 45 °C, giving CO as the main product, indicating the crucial role of LiCl (entry 9). The observed activity was compared with those of the reported catalysts. At 100 °C, the turnover number of CO (TON_{CO}) on Shvo's catalyst was more than 5 times that of either Ru₃(CO)₁₂ or [RuCl₂(CO)₃]₂ (entries S4–S6 in Table S1). Even at a 20 °C lower temperature, the activity of Shvo's catalyst was approximately twice that of [PPN][RuCl₃(CO)₃], which was claimed as the most efficient homogeneous catalyst for low-temperature RWGS^{7c} (TON_{CO}: 89 at 120 °C vs 43 at 140 °C; entry S16).

The reaction conditions were briefly screened, and the TON_{CO} increased with the increase of reaction temperature from 45 to 120 °C (entries 2 and 9–12). The effect from the stoichiometry of the alkali salt on the reaction was evaluated. The optimal ratio of LiCl/Ru at 60 °C is *ca.* 2 (Figure S1). Increasing pressure leads to a higher gas solubility and reaction rate, which results in higher efficiency of CO production (entries 12 and 14 and Figure S2a). The concentration of Shvo's catalyst is the other major concern (entries 15 and 16). By decreasing the concentration of the catalyst to 0.001 mol/L, the value of TON_{CO} could attain 290, while the selectivity toward CO was sustained above 99%. Amide solvents, such as NMP, *N*-ethyl-2-pyrrolidone, DMF, and *N,N*-dimethylacetamide, were superior to other solvents (Figure S2b).¹⁵ When further elevating the reaction temperature to 140 or 160 °C but reducing the concentration of Shvo's catalyst (0.001 mol/L), this set of catalyst–promoter combinations still exhibited remarkable catalytic performance with high CO selectivity (entries 17 and 18). The value of TON_{CO} could reach 1555 when the reaction temperature was increased to 160 °C.

The significant activity enhancement of Shvo's catalyst with the addition of LiCl led us to survey the role of Li⁺ and Cl⁻ ions. To assess the effect from Li⁺, complex 3 possessing the Cl⁻ ligand was prepared¹⁶ and applied into the CO₂ hydrogenation (Figure 1). It was almost inactive with a TON_{CO} of only 4. Adding LiCl dramatically increased the

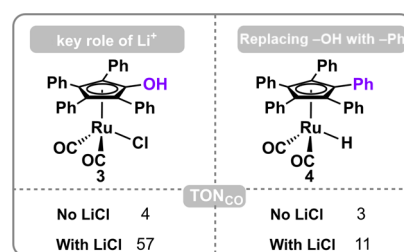


Figure 1. Indispensability of LiCl and the OH group of the ligand to RWGS activity (^creactions with 0.05 mmol Ru, 1 mL of NMP, 3 MPa CO₂, 3 MPa H₂, 120 °C, 10 h. All results represent the average values of the results for three runs).

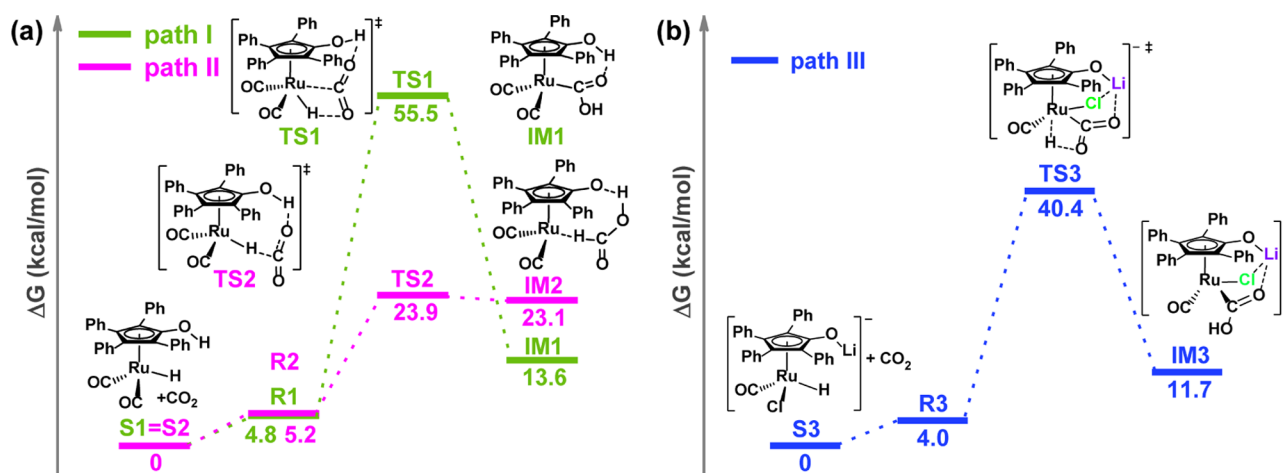


Figure 2. Free-energy profile with considering implicit solvation for the different manners of inserting CO₂ into the Ru–H bond: (a) forming Ru–CO₂H and Ru–formate in the absence of LiCl; (b) forming Ru–CO₂H in the presence of LiCl.

activity. This contrast revealed the critical role of Li⁺ in the conversion of CO₂ to CO. The Cl[−] anion was essential to the catalytic system, with only deficient performance in facilitating CO generation being found when Cl[−] was replaced with AcO[−], NO₃[−], HO[−], or CO₃^{2−} (Figure S4). The results also indicated that the effect of the alkali metal salt was unrelated to its alkaline nature. The acidic proton on the hydroxycyclopentadienyl ligand was suspected to be related to the high RWGS activity. Accordingly, by replacing the hydroxyl group with the phenyl substituent, complex 4 was synthesized¹⁷ for comparing with Shvo's catalyst. As expected, the TON_{CO} dropped from 89 to 11 even in the presence of LiCl when applying complex 4 as the catalyst. These patterns suggested the indispensability of both Li⁺ and Cl[−] ions to the activity of Shvo's catalyst for RWGS and further demonstrated the collaboration between Shvo's catalyst and the LiCl additive.

By the tool of DFT-based computation,¹¹ the cooperation of Shvo's catalyst with the LiCl additive for switching the selectivity of CO₂ hydrogenation was elucidated by comparing the scenarios with and without LiCl (Figure 2). The activation of CO₂ and the heterolytic cleavage of H₂ are the key steps during the hydrogenation of CO₂. Revealed by DFT results (Figure S6), the relative energy barrier of H₂ splitting (15.6 kcal/mol) was significantly lower than that of CO₂ activation (55.5 kcal/mol), indicating that the CO₂ activation should be the rate-determining step. This energy pattern is also consistent with the previous reports.^{8b,18} Concerning the CO₂ activation, the distinct manner for inserting CO₂ into the Ru–H bond results in two plausible paths. One is *via* affording the Ru–formate intermediate, which would lead the selectivity toward HCOOH through an “outer-sphere” hydrogenation mechanism.^{10a,19} The other is *via* generating the Ru–COOH intermediate, which further undergoes protonation and dehydration to afford CO.¹⁸ The computational outcomes show that in the absence of LiCl, generating HCOOH starting from the reaction between charge-neutral active species S1²⁰ and CO₂ *via* path II through Ru–formate intermediate IM2 was much more favorable than producing CO along path I through Ru–CO₂H intermediate IM1 (23.9 and 55.5 kcal/mol, respectively, Figures 2a and S7). The priority of yielding IM2 can be attributed to the H-bonding interaction between the hydroxyl group of the ligand and the oxygen of CO₂.^{10a}

Consequently, in the absence of LiCl, HCOOH would be the dominant product (Table 1, entry 1).

In contrast, the presence of LiCl drastically mitigated the resistance of Ru–CO₂H intermediate IM3 in path III heading to CO, which was affirmed by the significantly diminished energy barrier (Figure 2b). *Via* substituting the acidic proton on the hydroxycyclopentadienyl ligand and a carbonyl ligated to the Ru^{II} center respectively with Li⁺ and Cl[−], Shvo's catalyst was transformed to the anionic active species S3. The coordination with Cl[−] instead of CO enhances the nucleophilicity of Ru-hydride, which changes to the manner of CO₂ insertion into Ru–H (the detailed natural charge analysis of S1, S3, TS1, and TS3; see Figure S8).²¹ These outcomes showed that the presence of the LiCl additive indeed imposes effects on the chemoselectivity of CO₂ hydrogenation by altering the mechanism.

A plausible mechanism based on these experimental and theoretical studies is proposed (Scheme 2). Initially, complex 2 is *in situ* generated *via* the splitting of Shvo's catalyst in the presence of H₂. Afterward, Ru–H complex S3 is afforded *via* the substitution of the carbonyl ligand with LiCl. *Via* TS3, the insertion of CO₂ into the Ru–H bond affords IM3. After CO₂ activation, the dehydration of IM3 gives intermediate 5. Through the dissociation of carbonyl, the undercoordinated intermediate 6 is formed. Finally, *via* the heterolytic splitting of H₂ on intermediate 6 and the exchanging between the proton of the hydroxy group and Li⁺ (6 → 7 → 8 → S3), the active species is regenerated.

To validate the proposed mechanism, we attempted to obtain intermediate 5 and investigate its reactivity of RWGS. Fortunately, intermediate 5 was air-stable enough to be prepared *via* the reaction of either Shvo's catalyst or complex 2 with LiCl under a N₂ atmosphere (for the detailed procedure, see Section 2.1). Intermediate 5 in the NMP-solvated dimeric form was characterized by X-ray crystallography (Figures 3a and S10).²² More importantly, under the optimal conditions for the CO₂ hydrogenation to CO with a higher loading of Shvo's catalyst, intermediate 5 was detected and isolated (for the detailed procedure, see Section 2.3). At the same time, we also observed the other molecular ion peak with an *m/z* of 540.0210 (Figure 3c), which can be attributed to the anionic moiety of intermediate 6 formed *via* one carbonyl ligand dissociating from intermediate 5. To verify the

in switching the chemoselectivity from generating HCOOH to CO.

■ ASSOCIATED CONTENT

Supporting Information

The Supporting Information is available free of charge at <https://pubs.acs.org/doi/10.1021/acscatal.1c01874>.

General information, synthesis of catalysts, additional data of CO₂ hydrogenation, and XYZ coordinates for the critical transition states on DFT calculations (PDF)

Crystallography data of compounds (CIF)

■ AUTHOR INFORMATION

Corresponding Authors

Gangli Zhu – State Key Laboratory for Oxo Synthesis and Selective Oxidation (OSSO), Suzhou Research Institute of LICP, Lanzhou Institute of Chemical Physics (LICP), Chinese Academy of Sciences (CAS), Lanzhou 730000, China; University of Chinese Academy of Sciences, Beijing 100049, China; orcid.org/0000-0001-5148-762X; Email: zhugl@licp.cas.cn

Chun-Lin Lv – School of Pharmacy and Center on Translational Neuroscience, Minzu University of China, Beijing 100081, China; Email: chunlinlv@muc.edu.cn

Lin He – State Key Laboratory for Oxo Synthesis and Selective Oxidation (OSSO), Suzhou Research Institute of LICP, Lanzhou Institute of Chemical Physics (LICP), Chinese Academy of Sciences (CAS), Lanzhou 730000, China; University of Chinese Academy of Sciences, Beijing 100049, China; Dalian National Laboratory for Clean Energy, CAS, Dalian 116023, China; orcid.org/0000-0001-7437-1443; Email: helin@licp.cas.cn

Authors

Qiongyao Chen – State Key Laboratory for Oxo Synthesis and Selective Oxidation (OSSO), Suzhou Research Institute of LICP, Lanzhou Institute of Chemical Physics (LICP), Chinese Academy of Sciences (CAS), Lanzhou 730000, China; University of Chinese Academy of Sciences, Beijing 100049, China

Chaoren Shen – State Key Laboratory for Oxo Synthesis and Selective Oxidation (OSSO), Suzhou Research Institute of LICP, Lanzhou Institute of Chemical Physics (LICP), Chinese Academy of Sciences (CAS), Lanzhou 730000, China; School of Chemistry and Molecular Engineering, East China Normal University, Shanghai 200062, China; orcid.org/0000-0002-2849-7990

Xuehua Zhang – State Key Laboratory for Oxo Synthesis and Selective Oxidation (OSSO), Suzhou Research Institute of LICP, Lanzhou Institute of Chemical Physics (LICP), Chinese Academy of Sciences (CAS), Lanzhou 730000, China

Bo Zeng – State Key Laboratory for Oxo Synthesis and Selective Oxidation (OSSO), Suzhou Research Institute of LICP, Lanzhou Institute of Chemical Physics (LICP), Chinese Academy of Sciences (CAS), Lanzhou 730000, China

Sen Wang – State Key Laboratory of Coal Conversion, Institute of Coal Chemistry, Chinese Academy of Sciences, Taiyuan 030001, China

Junfen Li – Dalian National Laboratory for Clean Energy, CAS, Dalian 116023, China; State Key Laboratory of Coal

Conversion, Institute of Coal Chemistry, Chinese Academy of Sciences, Taiyuan 030001, China

Weibin Fan – State Key Laboratory of Coal Conversion, Institute of Coal Chemistry, Chinese Academy of Sciences, Taiyuan 030001, China; orcid.org/0000-0001-7362-0348

Complete contact information is available at:

<https://pubs.acs.org/doi/10.1021/acscatal.1c01874>

Author Contributions

The manuscript was written through contributions of all authors. All authors have given approval to the final version of the manuscript. Q.C. and C.S. contributed equally.

Funding

The Dalian National Laboratory for Clean Energy (DNL) Cooperation Fund, the CAS (DNL201919), the National Natural Science Foundation of China (nos. 21802151, 21972152, and 21802152), the Natural Science Foundation of the Jiangsu Higher Education Institutions of China (BK20180249), the Key Research Program of Frontier Sciences of CAS (QYZDJ-SSW-SLH051), and the Youth Innovation Promotion Association of CAS (2018453) are acknowledged.

Notes

The authors declare no competing financial interest.

■ ACKNOWLEDGMENTS

L.H. would like to thank the Dalian National Laboratory for Clean Energy (DNL) Cooperation Fund and the CAS (DNL201919). This work was financially supported by the National Natural Science Foundation of China (nos. 21802151, 21972152, and 21802152) and the Natural Science Foundation of the Jiangsu Higher Education Institutions of China (BK20180249). L.H. and G.Z. also acknowledge the grant from the Key Research Program of Frontier Sciences of CAS (QYZDJ-SSW-SLH051) and the Youth Innovation Promotion Association of CAS (2018453).

■ REFERENCES

- (1) (a) Weillhard, A.; Argent, S. P.; Sans, V. Efficient Carbon Dioxide Hydrogenation to Formic Acid with Buffering Ionic Liquids. *Nat. Commun.* **2021**, *12*, 231–237. (b) Sordakis, K.; Tang, C.; Vogt, L. K.; Junge, H.; Dyson, P. J.; Beller, M.; Laurenczy, G. Homogeneous Catalysis for Sustainable Hydrogen Storage in Formic Acid and Alcohols. *Chem. Rev.* **2017**, *118*, 372–433.
- (2) (a) Nielsen, D. U.; Hu, X.-M.; Daasbjerg, K.; Skrydstrup, T. Chemically and Electrochemically Catalysed Conversion of CO₂ to CO with Follow-up Utilization to Value-added Chemicals. *Nat. Catal.* **2018**, *1*, 244–254. (b) Klankermayer, J.; Wesselbaum, S.; Beydoun, K.; Leitner, W. Selective Catalytic Synthesis Using the Combination of Carbon Dioxide and Hydrogen: Catalytic Chess at the Interface of Energy and Chemistry. *Angew. Chem., Int. Ed.* **2016**, *55*, 7296–7343.
- (3) (a) Zhong, J.; Yang, X.; Wu, Z.; Liang, B.; Huang, Y.; Zhang, T. State of the Art and Perspectives in Heterogeneous Catalysis of CO₂ Hydrogenation to Methanol. *Chem. Soc. Rev.* **2020**, *49*, 1385–1413. (b) Zhu, Y.; Zheng, J.; Ye, J.; Cui, Y.; Koh, K.; Kovarik, L.; Camaioni, D. M.; Fulton, J. L.; Truhlar, D. G.; Neurock, M.; Cramer, C. J.; Gutiérrez, O. Y.; Lercher, J. A. Copper-Zirconia Interfaces in UiO-66 Enable Selective Catalytic Hydrogenation of CO₂ to Methanol. *Nat. Commun.* **2020**, *11*, 5849–5859.
- (4) (a) Cored, J.; García-Ortiz, A.; Iborra, S.; Climent, M. J.; Liu, L.; Chuang, C.-H.; Chan, T.-S.; Escudero, C.; Concepción, P.; Corma, A. Hydrothermal Synthesis of Ruthenium Nanoparticles with a Metallic Core and a Ruthenium Carbide Shell for Low-Temperature

Activation of CO₂ to Methane. *J. Am. Chem. Soc.* **2019**, *141*, 19304–19311. (b) Kato, S.; Matam, S. K.; Kerger, P.; Bernard, L.; Battaglia, C.; Vogel, D.; Rohwerder, M.; Züttel, A. The Origin of the Catalytic Activity of a Metal Hydride in CO₂ Reduction. *Angew. Chem., Int. Ed.* **2016**, *55*, 6028–6032.

(5) (a) Zhu, M.; Ge, Q.; Zhu, X. Catalytic Reduction of CO₂ to CO via Reverse Water Gas Shift Reaction: Recent Advances in the Design of Active and Selective Supported Metal Catalysts. *Trans. Tianjin Univ.* **2020**, *26*, 172–187. (b) Zhu, M.; Tian, P.; Ford, M. E.; Chen, J.; Xu, J.; Han, Y.-F.; Wachs, I. E. Nature of Reactive Oxygen Intermediates on Copper-Promoted Iron-Chromium Oxide Catalysts during CO₂ Activation. *ACS Catal.* **2020**, *10*, 7857–7863.

(6) (a) Liu, Q.; Wu, L.; Jackstell, R.; Beller, M. Using Carbon Dioxide as a Building Block in Organic Synthesis. *Nat. Commun.* **2015**, *6*, 5933–5947. (b) Artz, J.; Müller, T. E.; Thenert, K.; Kleinekorte, J.; Meys, R.; Sternberg, A.; Bardow, A.; Leitner, W. Sustainable Conversion of Carbon Dioxide: An Integrated Review of Catalysis and Life Cycle Assessment. *Chem. Rev.* **2018**, *118*, 434–504. (c) Cao, Y.; Yang, J. G.; Deng, Y.; Wang, S.; Liu, Q.; Shen, C.; Lu, W.; Che, C. M.; Chen, Y.; He, L. Amine-Responsive Disassembly of Au^I-Cu^I Double Salts for Oxidative Carbonylation. *Angew. Chem., Int. Ed.* **2020**, *59*, 2080–2084. (d) Cui, M.; Qian, Q.; Zhang, J.; Wang, Y.; Asare Bediako, B. B.; Liu, H.; Han, B. Liquid fuel Synthesis via CO₂ Hydrogenation by Coupling Homogeneous and Heterogeneous Catalysis. *Chem* **2021**, *7*, 726–737. (e) Zhang, X.; Shen, C.; Xia, C.; Tian, X.; He, L. Alkoxy carbonylation of Olefins with Carbon Dioxide by a Reusable Heterobimetallic Ruthenium–cobalt Catalytic System. *Green Chem.* **2018**, *20*, 5533–5539. (f) Liu, Q.; Wu, L.; Fleischer, I.; Selent, D.; Franke, R.; Jackstell, R.; Beller, M. Development of a Ruthenium/Phosphite Catalyst System for Domino Hydroformylation-Reduction of Olefins with Carbon Dioxide. *Chem.—Eur. J.* **2014**, *20*, 6888–6894.

(7) (a) Su, X.; Yang, X.; Zhao, B.; Huang, Y. Designing of Highly Selective and High-temperature Endurable RWGS Heterogeneous Catalysts: Recent Advances and the Future Directions. *J. Energy Chem.* **2017**, *26*, 854–867. (b) Tominaga, K.-i.; Sasaki, Y.; Hagihara, K.; Watanabe, T.; Saito, M. Reverse Water-Gas Shift Reaction Catalyzed by Ruthenium Cluster Anions. *Chem. Lett.* **1994**, *23*, 1391–1394. (c) Tsuchiya, K.; Huang, J.-D.; Tominaga, K.-i. Reverse Water-Gas Shift Reaction Catalyzed by Mononuclear Ru Complexes. *ACS Catal.* **2013**, *3*, 2865–2868. (d) Li, S.; Xu, Y.; Chen, Y.; Li, W.; Lin, L.; Li, M.; Deng, Y.; Wang, X.; Ge, B.; Yang, C.; Yao, S.; Xie, J.; Li, Y.; Liu, X.; Ma, D. Tuning the Selectivity of Catalytic Carbon Dioxide Hydrogenation over Iridium/Cerium Oxide Catalysts with a Strong Metal-Support Interaction. *Angew. Chem., Int. Ed.* **2017**, *56*, 10761–10765. (e) Yasuda, T.; Uchiage, E.; Fujitani, T.; Tominaga, K.-i.; Nishida, M. Reverse Water Gas Shift Reaction Using Supported Ionic Liquid Phase Catalysts. *Appl. Catal., B* **2018**, *232*, 299–305.

(8) (a) Jessop, P. G.; Ikariya, T.; Noyori, R. Homogeneous Hydrogenation of Carbon Dioxide. *Chem. Rev.* **1995**, *95*, 259–272. (b) Schneck, F.; Ahrens, J.; Finger, M.; Stückl, A. C.; Würtele, C.; Schwarzer, D.; Schneider, S. The Elusive Abnormal CO₂ Insertion Enabled by Metal-Ligand Cooperative Photochemical Selectivity Inversion. *Nat. Commun.* **2018**, *9*, 1161–1167.

(9) (a) Matsubara, T. Promotion Effect of the Protonated Amine Arm of a Ruthenium Complex on Hydrido Migration to CO₂: A Density Functional Study. *Organometallics* **2001**, *20*, 19–24. (b) Singh Rawat, K.; Garg, P.; Bhauriyal, P.; Pathak, B. Metal-ligand bifunctional based Mn-catalysts for CO₂ Hydrogenation Reaction. *Mol. Catal.* **2019**, *468*, 109–116.

(10) (a) Hou, C.; Jiang, J.; Zhang, S.; Wang, G.; Zhang, Z.; Ke, Z.; Zhao, C. Hydrogenation of Carbon Dioxide Using Half-Sandwich Cobalt, Rhodium, and Iridium Complexes: DFT Study on the Mechanism and Metal Effect. *ACS Catal.* **2014**, *4*, 2990–2997. (b) Ge, H.; Chen, X.; Yang, X. Hydrogenation of Carbon Dioxide to Methanol Catalyzed by Iron, Cobalt, and Manganese Cyclopentadienone Complexes: Mechanistic Insights and Computational Design. *Chem.—Eur. J.* **2017**, *23*, 8850–8856. (c) Ge, H.; Chen, X.; Yang, X. A Mechanistic Study and Computational Prediction of Iron,

Cobalt and Manganese Cyclopentadienone Complexes for Hydrogenation of Carbon Dioxide. *Chem. Commun.* **2016**, *52*, 12422–12425.

(11) Frisch, M. J.; et al. *Gaussian 16*, Revision C.01; Gaussian Inc.: Wallingford CT, 2016. See the [Supporting Information](#) for the full citation.

(12) Chiodo, S.; Russo, N.; Sicilia, E. LANL2DZ Basis Sets Recontracted in the Framework of Density Functional theory. *J. Chem. Phys.* **2006**, *125*, 104107–104114.

(13) Marenich, A. V.; Cramer, C. J.; Truhlar, D. G. Universal Solvation Model Based on Solute Electron Density and on a Continuum Model of the Solvent Defined by the Bulk Dielectric Constant and Atomic Surface Tensions. *J. Phys. Chem. B* **2009**, *113*, 6378–6396.

(14) Dolg, M.; Stoll, H.; Preuss, H. A Combination of Quasirelativistic Pseudopotential and Ligand Field Calculations for Lanthanoid Compounds. *Theor. Chim. Acta* **1993**, *85*, 441–450.

(15) Wang, Y.; Zhang, J.; Qian, Q.; Asare Bediako, B. B.; Cui, M.; Yang, G.; Yan, J.; Han, B. Efficient Synthesis of Ethanol by Methanol Homologation Using CO₂ at Lower Temperature. *Green Chem.* **2019**, *21*, 589–596.

(16) Jung, H. M.; Choi, J. H.; Lee, S. O.; Kim, Y. H.; Park, J. H.; Park, J. Facile Synthesis of (η^5 -Ph₄C₄COH)(CO)₂RuCl and Catalytic Oxidation of Alcohols with Chloroform. *Organometallics* **2002**, *21*, 5674–5677.

(17) (a) Field, L. D.; Ho, K. M.; Lindall, C. M.; Masters, A. E.; Webb, A. G. The Preparation and Characterization of Substituted Pentaphenylcyclopentadienyl Ligands, Their Precursors, and Complexes of Iron. *Aust. J. Chem.* **1990**, *43*, 281–291. (b) Pinggen, D.; Altıntaş, Ç.; Rudolf Schaller, M.; Vogt, D. A Ruthenium Racemisation Catalyst for the Synthesis of Primary Amines from Secondary Amines. *Dalton Trans.* **2016**, *45*, 11765–11771.

(18) Zhang, X.; Tian, X.; Shen, C.; Xia, C.; He, L. Acid-Promoted Hydroformylative Synthesis of Alcohol with Carbon Dioxide by Heterobimetallic Ruthenium-Cobalt Catalytic System. *ChemCatChem* **2019**, *11*, 1986–1992.

(19) Hu, J.; Bruch, Q. J.; Miller, A. J. M. Temperature and Solvent Effects on H₂ Splitting and Hydricity: Ramifications on CO₂ Hydrogenation by a Rhenium Pincer Catalyst. *J. Am. Chem. Soc.* **2021**, *143*, 945–954.

(20) Gusev, D. G.; Spasyuk, D. M. Revised Mechanisms for Aldehyde Disproportionation and the Related Reactions of the Shvo Catalyst. *ACS Catal.* **2018**, *8*, 6851–6861.

(21) Liu, Z.; Jiang, W.; Liu, Z.; Wang, Y.; Wang, D.; Hao, D.; Yao, W.; Teng, F. Optimizing the Carbon Dioxide Reduction Pathway through Surface Modification by Halogenation. *ChemSusChem* **2020**, *13*, 5638–5646. (b) Geboes, Y.; Nagels, N.; Pinter, B.; De Profit, F.; Herrebout, W. A. Competition of C(sp²)-X...O Halogen Bonding and Lone Pair... π Interactions: Cryospectroscopic Study of the Complexes of C₂F₃X (X = F, Cl, Br, and I) and Dimethyl Ether. *J. Phys. Chem. A* **2015**, *119*, 2502–2516.

(22) CCDC 2076363 contains the supplementary crystallographic data for this paper. These data can be obtained free of charge via www.ccdc.cam.ac.uk/conts/retrieving.html.

(23) Casey, C. P.; Singer, S. W.; Powell, D. R.; Hayashi, R. K.; Kavana, M. Hydrogen Transfer to Carbonyls and Imines from a Hydroxycyclopentadienyl Ruthenium Hydride: Evidence for Concerted Hydride and Proton Transfer. *J. Am. Chem. Soc.* **2001**, *123*, 1090–1100.